EARTH SURFACE PROCESSES AND LANDFORMS
Earth Surf. Process. Landforms **34**, 291–304 (2009)

Published online 9 December 2008 in Wiley InterScience
(www.interscience.wiley.com) DOI: 10.1002/esp.1725

Floodplain development in an engineered setting

Michael Bliss Singer[1,2]* and Rolf Aalto[3,4]
[1] School of Geography and Geosciences, University of St Andrews, St Andrews, Fife, UK
[2] Institute for Computational Earth System Science, University of California Santa Barbara, Santa Barbara, CA, USA
[3] Department of Geography, Archaeology, and Earth Resources, University of Exeter, Exeter, UK
[4] Department of Earth and Space Sciences, University of Washington, Seattle, WA, USA

Received 25 February 2008; Revised 20 May 2008; Accepted 2 June 2008

* Correspondence to: Michael Bliss Singer, Institute for Computational Earth System Science, University of California Santa Barbara, Santa Barbara, CA, USA. E-mail: bliss@icess.ucsb.edu

ESPL
Earth Surface Processes and Landforms

ABSTRACT: Engineered flood bypasses, or simplified conveyance floodplains, are natural laboratories in which to observe floodplain development and therefore present an opportunity to assess delivery to and sedimentation within a specific class of floodplain. The effects of floods in the Sacramento River basin were investigated by analyzing hydrograph characteristics, estimating event-based sediment discharges and reach erosion/deposition through its bypass system and observing sedimentation patterns with field data. Sediment routing for a large, iconic flood suggests high rates of sedimentation in major bypasses, which is corroborated by data for one bypass area from sedimentation pads, floodplain cores and sediment removal reporting from a government agency. These indicate a consistent spatial pattern of high sediment accumulation both upstream and downstream of lateral flow diversions and negligible sedimentation in a 'hydraulic shadow' directly downstream of a diversion weir. The pads located downstream of the shadow recorded several centimeters of deposition during a moderate flood in 2006, increasing downstream to a peak of ~10 cm thick and thinning rapidly thereafter. Flood deposits in the sediment cores agree with this spatial pattern, containing discrete sedimentation layers (from preceding floods) that increase in thickness with distance downstream of the bypass entrance to several decimeters thick at the peak and then thin downstream. These patterns suggest that a quasi-natural physical process of levee construction by advective overbank transport and deposition of sediment is operating. The results improve understanding of the evolution of bypass flood control structures, the transport and deposition of sediment within these environments and the evolution of one class of natural levee systems. Copyright © 2008 John Wiley & Sons, Ltd.

KEYWORDS: floodplain sedimentation; bypasses; floods; natural levees; 210-Pb geochronology

Introduction

In large river systems, fine sediment transport and deposition patterns are often affected by engineered channel constraints designed for flood conveyance or navigation. Such managed channels have a limited number of overflow loci through which suspended sediment can enter the river's floodplain. Engineered flood bypasses along the Sacramento River are narrow relict floodplains that are accessed by lateral overflow weirs (Figure 1) in order to convey high discharges out of the trunk stream. Although they represent simplified floodplains and thus may offer new insight into natural floodplain development, little is known about spatial and temporal patterns and processes of sedimentation in bypasses. Like natural floodplains, bypasses are net sinks of fine sediment from the main channel. However, they contain contemporary sedimentation records that are likely to differ from those of the various natural floodplains (see, e.g., Nanson and Croke, 1992), due to their constricted geometry, stability of channel location, regulated flow, frequency of sediment delivery and processes of floodplain sedimentation and scour around engineered structures. Flood bypasses represent an end-member case of advective hydraulic delivery to, and sediment accumulation within, a conveyance floodplain characterized by maximum transport efficiently and minimum storage for floodwaters. In this paper we investigate sediment movement into these bypasses and the resulting spatial and temporal patterns of sediment storage and remobilization in a data-rich flood bypass system in California.

Studies of overbank sediment deposition on floodplains are motivated by the general observation that significant quantities of fine sediment are stored in alluvial valleys (see, e.g., Trimble, 1974). Prior investigations have analyzed event-based sedimentation patterns via sediment traps (Walling and Bradley, 1989; Asselman and Middelkoop, 1995; Middelkoop and Asselman, 1998), post-flood measurements (Stewart and LaMarche, 1967; Kesel *et al.*, 1974; Gomez *et al.*, 1997; Ten Brinke *et al.*, 1998), and dating fallout radionuclides from sediment cores on decadal and annual timescales (He and Walling, 1996; Goodbred and Kuehl, 1998; Siggers *et al.*, 1999; Walling, 1999; Aalto, 2002; Aalto *et al.*, 2003, 2008; Swanson *et al.*, 2008).

This research builds upon previous work by assessing depositional patterns within an engineered floodplain setting via sediment pads after a flood and via ^{210}Pb geochronology. It also complements a decadal suspended load budget for the main-stem Sacramento (Singer and Dunne, 2001). The latter research used time series analysis to relate daily mean discharge to daily mean sediment concentration in order to

Figure 1. Oblique aerial photograph over Colusa Weir and Colusa Bypass with the Sacramento River in the background. During floods stage rises in the Sacramento until flow overtops the concrete weir (under the bridge) and moves east (down in the photo) into the bypass system. The flow first enters Colusa Bypass, then Butte Basin, before entering Sutter Bypass (not shown).

extend the sediment record over a 32-year period, and to quantify net erosion/deposition in long reaches throughout the main-stem Sacramento River. However, that study did not assess sediment transport during individual extreme flooding periods, which is necessary to determine the impact of episodic flooding on sediment accumulation within the Sacramento bypasses.

In the event-based study presented herein, we provide new data and analysis for the impact of individual large floods on sedimentation in the bypass system. We first develop a suspended load routing analysis for an iconic flood event within the larger system, which accentuates the role of bypasses as system depocenters for sediment transported by Sacramento Valley trunk streams. We then focus on the largest of these bypasses, using data from various sources and time periods to characterize event-based sedimentation patterns in these simplified floodplains. We model daily suspended load efflux over each weir and daily transport at various gauging stations in and around the bypass system during a single large hydrologic event for which the fullest range of data are available for streamflow, sediment concentration and flood hydraulics. We also analyze the flood hydrograph, assess net erosion/sedimentation through the study reach and describe bypass deposition based on data from sedimentation pads that recorded deposition during a recent large flood and from sediment cores that were dated using ^{210}Pb and analyzed for grain size.

We present the effect of floods on bypass sediment delivery, scour and sedimentation and address the problem of particle sorting once sediment enters a bypass (or floodplain characterized by the mechanism of advective transport away from the channel). Ultimately we address the question of where and when should we expect floodplain sedimentation and/or scour within bypass systems. The results of this research have implications for quantifying storage of fines, for predicting the fate of contaminants (such as mercury and pesticides) that might be adsorbed to fine sediments, for assessing the long-term functioning of engineered flood control systems and for modeling scenarios of habitat restoration (see, e.g., Singer and Dunne, 2006) in large, engineered conveyance floodplains that provide flood control, while supporting agriculture and complex aquatic and riparian habitats (Sommer *et al.*, 2001a, 2001b, 2004).

Study Area

The Sacramento Valley comprises the northern half of California's Central Valley and is drained by the Sacramento River, which contributes to the San Francisco Bay-Delta. Under natural conditions (i.e. before floodplain development), the Sacramento River had insufficient capacity to convey winter and spring floods (US Army Corps of Engineers, 1965; James and Singer, 2008; Singer *et al.*, 2008). The frequency of large floods, which predated hydraulic mining (US Army Corps of Engineers, 1965; Kelley, 1998), ultimately led to the development of a flood control plan that used portions of the existing flood basins as bypass conveyance channels for high flows (the report of engineers M. Manson and C. E. Grunsky is outlined in a document of the US House of Representatives (1911)). Although dams were also built in a subsequent phase of development, the Sacramento Valley is still reliant on the bypass system for its flood control (Singer, 2007). In his assessment of the proposed flood control system, Gilbert (1917) noted that, although large amounts of sediment had accumulated in the flood basins, if the bypass channels were designed with appropriate slope then flow velocities would be high enough to maintain the bypasses in the historic flood basins as self-scouring channels. This paper evaluates Gilbert's expectation at selected sites under measured and modeled flood conditions with data collected since the bypasses were constructed.

The study is focused on flow and sediment dispersal into the Sacramento Valley bypass system, which is served by four primary passive weirs (Moulton, Colusa, Tisdale and Fremont), two minor bypass channels, Colusa and Tisdale, and two major bypass channels, Sutter and Yolo (Figure 2). Sacramento Weir is an active weir (i.e. it has operational gates) upstream of the city of Sacramento, which is not treated in this study because it delivers its sediment load to Yolo Bypass downstream of our focus area. Flood flow over Moulton and Colusa Weirs enters Butte Basin and subsequently Sutter Bypass, augmented by Tisdale Weir and the Feather River. The latter, which drains the Sierra Nevada, mixes during floods with Sutter Bypass flow due to a backwater that forms at the Feather's confluence with the main-stem Sacramento. Due to the low channel capacity at this confluence, located downstream of Fremont Weir, most of the Sutter Bypass flood discharge passes over Fremont Weir

DOI: 10.1002/esp

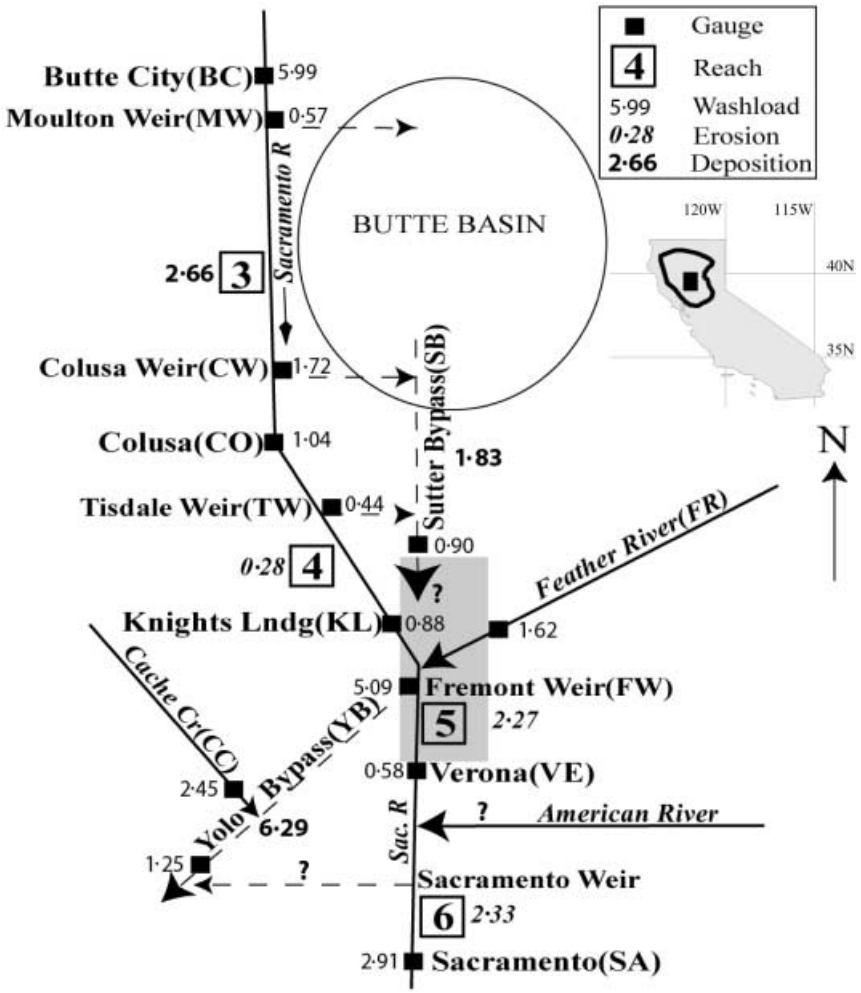

Figure 2. Schematic map of the lower Sacramento River and bypass system, including main channel, tributaries, flood diversions and bypass channels. Event-based sediment discharge for the 1964 flood was computed for each station and net erosion/deposition are shown for each reach. Due to lack of data, computations have not been carried out for the southern end of Sutter Bypass, the American River and Sacramento Weir (question marks). Therefore, for Sutter Bypass the load of 0.9 megatonnes is used in the sediment budget calculations for Reach 5 (Table III). The large gray rectangle represents Reach 5. All values are expressed in megatonnes. Not to scale. Inset: the basin boundary is outlined in black and the study area is in the black box.

into Yolo Bypass (Singer *et al.*, 2008). Yolo Bypass receives additional flow from Cache Creek, which drains part of the Coast Range, before reaching the downstream extent of our study area (in the bypass system). However, much of the sediment measured at the Cache Creek gauge is trapped in a settling basin upstream of the Yolo Bypass confluence.

We utilized flow and sediment concentration data from 13 gauging stations in and around the bypass system (Figure 2) to assess the impact of a single, large flood on suspended load transport to and storage within flood bypasses. We then focus the discussion on the entrance of Yolo Bypass, for which we provide various sources of data to investigate sedimentation patterns.

The Modeled Flood

The iconic flood of 1964–1965 (hereafter referred to as 1964) had a large effect on the Sacramento River basin (US Army Corps of Engineers, 1965). Two consecutive storm systems produced a double-peaked flood (Figure 3) via a retrogression of a high-pressure ridge between the southeastern Pacific and the Aleutian Islands (i.e. the Pacific High) (Waananen *et al.*, 1971). It occurred during anomalous thermal circulation and pressure patterns of cold-phase El Niño Southern Oscillation (ENSO) and the Pacific North American (PNA) teleconnection (Wallace and Gutzler, 1981). Herein we analyze suspended load, net erosion/deposition, and sedimentation patterns over the entire event (including both peaks).

We chose to model the 1964 event because it is the largest flood in the bypass system for which ample flow data exist – many gauging stations were later decommissioned. Although we utilize flow data from 1964 along with sediment rating curves (see below) developed from data collected mostly in the late 1970s, there are no apparent trends in annual suspended load in the basin for the period 1963–1979 ($R^2 = 0{\cdot}095$ and $p = 0{\cdot}229$, Singer and Dunne, 2001), substantiating this approach. The results from the 1964 flood analysis are likely indicative of flooding and sediment storage during similar large floods during and since this period.

Flood Hydrograph

Figure 3 shows 1964 flood hydrographs for all gauging stations in and around the bypass system (listed in Table I). It is apparent from these hydrographs that the bypass system had a large influence on flood flow at downstream gauges. For example, flow over Moulton, Colusa and Tisdale Weirs damped out main channel flow peaks at Knights Landing. The same is true

DOI: 10.1002/esp

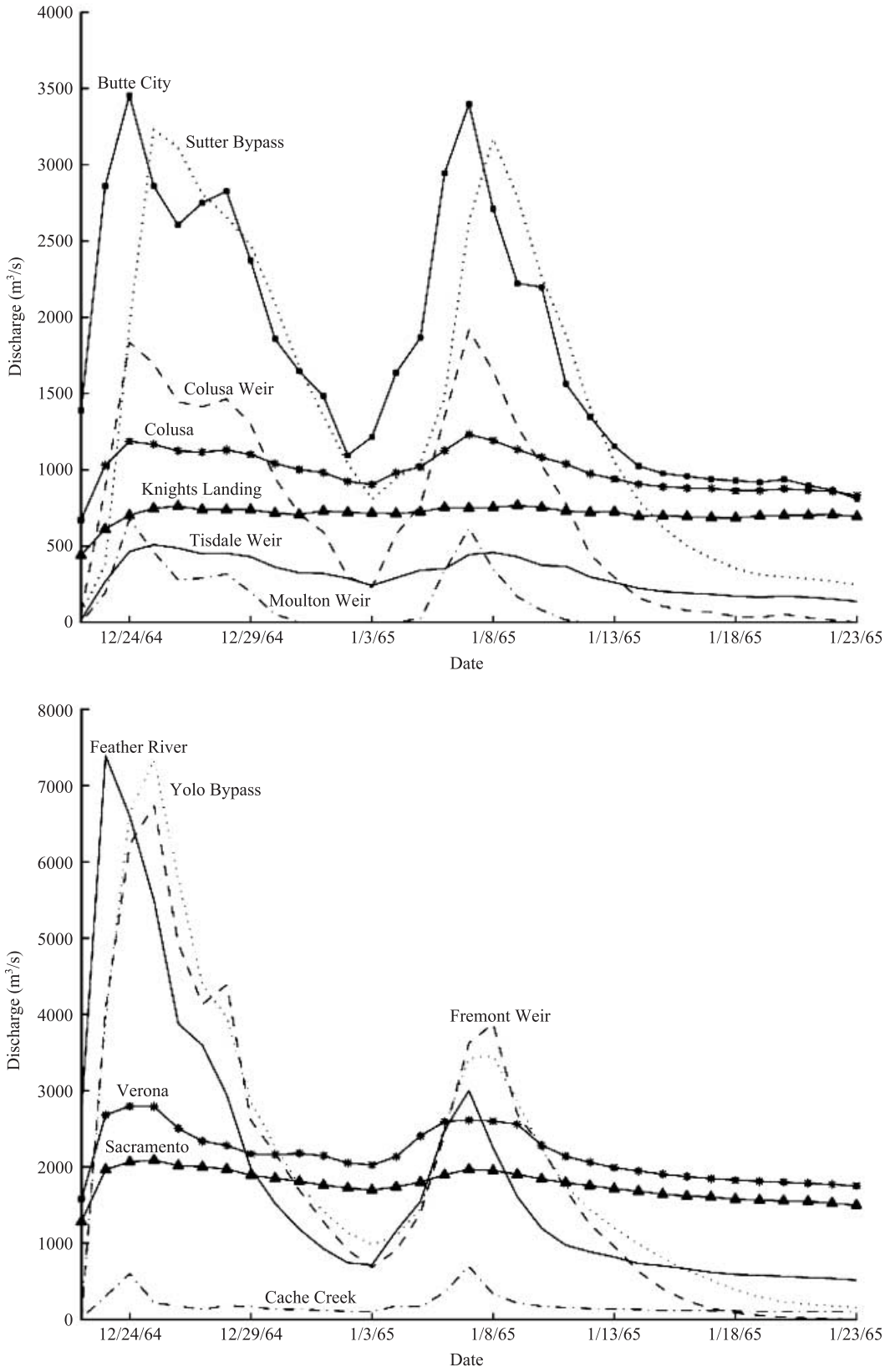

Figure 3. Daily mean flood hydrographs recorded during the 1964 flood at the 13 gauges listed in Table I. The upper panel is the upstream part of the bypass system and the lower panel is the downstream part. Lines with symbols indicate main-stem gauges. Note that the vertical scale doubles in the lower panel.

for the influence of Fremont Weir on flow at Verona. Also apparent from Figure 3 is the direct translation of the magnitude and shape of the Feather River hydrograph to Fremont Weir and Yolo Bypass (with a one-day phase shift), indicating that flood flow in Yolo Bypass is dominated by the flood signal from the Sierra Nevada.

We used daily mean flow records shown in Figure 3 for the periods of record shown in Table I to compute empirical plotting position exceedance probabilities (without curve fitting) for various hydrograph characteristics of the 1964 flood at each gauging station (Figure 2). We analyzed frequency of peak discharge (from the annual series), time to peak (computed as

DOI: 10.1002/esp

Table I. Flood characteristics and their respective exceedance probabilities at stations in and around the Sacramento bypass system. Cache Creek is tributary to Yolo Bypass and Feather River to the main-stem Sacramento. Columns are Station (including years of record and date flood weirs were completed – in square brackets), date of peak (the larger of the two 1964 event peaks), annual peak discharge, time to peak (days between baseline discharge and peak) and drawdown (days between peak and baseline discharge). Shaded rows refer to stations on the main-stem Sacramento

Station (Period)	Date	Peak Q (m^3/s)	Prob	Time to Peak[#] (d)	Prob	Drawdown[#] (d)	Prob
Butte City (1938–1994)	24/12/64	3455	0·20	3	0·28	56	0·03
Cache Creek (1903–2002)	23/12/64	603	0·09	3	0·46	88	0·13
Colusa (1940–2002)	24/12/64	1186	0·32	3	0·33	58	0·04
Colusa Weir [1933] (1943–1980)	24/12/64	1835	0·14	3	0·28	42	0·01
Feather River (1943–1983)	23/12/64	7391	0·05	3	0·32	71	0·04
Fremont Weir [1924] (1947–1975, 1984–2002)[&]	25/12/64	6740	0·05	4	0·42	42	0·03
Knights Landing (1940–1980)	26/12/64	762	0·42	5	0·29	62	0·08
Moulton Weir [1932] (1943–1977)	24/12/64	679	0·12	2	0·33	8	0·09
Sacramento (1948–2002)	24/12/64	2798	0·09	4	0·40	69	0·08
Sutter Bypass (1960–1980)	25/12/64	3228	0·10	6	0·25	43	0·02
Tisdale Weir [1932] (1943–1980)	25/12/64	509	0·38	4	0·30	50	0·02
Verona (1929–2002)	25/12/64	2090	0·15	4	0·45	68	0·07
Yolo Bypass (1939–2002)	25/12/64	7335	0·05	3	0·62	27	0·04

[#] Computed with reference to wet season baseline discharge (refer to Singer and Dunne, 2004).
[&] Gap in the flood record results from change-over in agency management.

number of days between a statistically determined baseline (Singer and Dunne, 2004) and the flood peak in a partial duration series) and drawdown (i.e. number of days between flood peak and the return to the baseline in a partial duration series).

Analysis of the event hydrograph and station statistics suggests that the majority of the flood was produced in the Sierra Nevada drained by the Feather River (Figure 3 and Table I), consistent with precipitation data (http://www.ncdc.noaa.gov) that plot the highest rainfall totals in Sierra tributary basins. However, most of the flood flow in the Feather River passed over Fremont Weir and into Yolo Bypass (Figure 3 and Table I), reducing flood peak probabilities in the main-stem Sacramento downstream of this confluence. Similar flood peak (and risk) reduction occurred in the upper part of the bypass system (Figure 3).

Consistent basin-wide patterns emerge from analysis of hydrograph shape during the 1964 event. Table I shows that time to peak was short (2–6 days) at all stations in and around the bypass system for the December peak. Drawdown after this peak, on the other hand, was atypically long (averaging well over a month) for all stations in the bypass system (exceedance probabilities range from 0·01 to 0·13) because the event had two peaks. These data suggest that large floods in the Sacramento basin are distinguished from small floods by their right-skewed hydrograph shape. Such prolonged floods can orchestrate substantial deposition, so long as sediment continues to be delivered downstream from hillslopes, in-channel scour and channel migration, and from the collapse of saturated banks.

Modeling Suspended Load and Net Storage

We determined daily flow depth over weir crest for each of the four weirs during flood spillage via discharge records and rating tables from CDWR. We computed sediment loads during the 1964 event for 10 of 13 stations using sediment rating curves that were developed from data acquired after the 1964 flood. Rating curves were developed from instantaneous discharges and associated sediment concentrations that were comparable to the 1964 flood (except Feather River, for which significant extrapolation was necessary, Tables I and II). Sediment concentrations from the 1964 flood exist for the Sacramento station, but no concentration data are available for any dates for the Moulton and Fremont Weir gauges.

Linear least squares regressions were constructed for log-transformed data (Table II). All residuals satisfied assumptions of homoscedasticity, independence and normality. We used

Table II. Sediment data used in the analysis. Columns are station (abbreviation from Figure 2), years of sediment concentration records, maximum discharge represented in regressions, number of observations used for regression (n), coefficient of determination (R^2), adjusted R^2, ANOVA F statistic (and p value of significance), logarithmic regression slope (and standard error, s.e.) and logarithmic regression intercept (and s.e.). MW, FW and SA are not present in this table because regressions were not constructed for these stations

Station	Years	Max Q (m^3)	n	R^2	Adj R^2	Fstat(p value)	Slope(s.e.)	Intercept(s.e.)
BC	1978–80	3455	19	0·80	0·78	$66·6(2·8 \times 10^{-7})$	1·36(·17)	–3·70(·72)
CC	1957–1986	850	126	0·63	0·63	$214·5(9·9 \times 10^{-29})$	0·60(·04)	1·12(·13)
CO	1973–99	1330	130	0·67	0·67	$264·0(6·7 \times 10^{-33})$	1·25(·08)	–3·22(·33)
CW	1973–79	1696	26	0·63	0·61	$40·4(1·4 \times 10^{-6})$	0·56(·09)	0·30(·37)
FR	1979–1996	3171	16	0·71	0·69	$34·8(3·9 \times 10^{-5})$	0·71(·12)	–1·21(·49)
KL	1978–80	821	24	0·78	0·77	$79·9(8·9 \times 10^{-9})$	1·34(·15)	–3·31(·63)
SB	1979–80	3455	13	0·55	0·51	$13·5(3·7 \times 10^{-3})$	0·74(·20)	–1·33(·94)
TW	1978–79	651	4	0·96	0·93	$42·9(2·3 \times 10^{-2})$	0·30(·05)	1·48(·19)
VE	1980–1998	2010	32	0·59	0·57	$42·8(3·1 \times 10^{-7})$	0·61(·09)	–0·89(·41)
YB	1957-1980	5267	34	0·58	0·57	$44·2(1·7 \times 10^{-7})$	0·15(·02)	1·56(·09)

DOI: 10.1002/esp

rating curves to relate instantaneous discharge to instantaneous sediment concentration (recently released). There are several potential problems associated with the use of rating curves that are discussed elsewhere (e.g. Ferguson, 1986; Asselman, 2000; Horowitz, 2003). Particularly relevant here are the difficulties associated with intra- and inter-flood hysteresis associated with sediment exhaustion and/or remobilization.

Regressions are generally good between concentration and discharge at main-stem stations. However, concentrations over Colusa and Tisdale Weirs exhibit strong seasonal hysteresis, which limits the utility of linear regressions. Regressions using data only from late December and January (the time period of the 1964 event and other major Sacramento Valley floods) at these stations exhibited statistically better fits (e.g. from adjusted R^2 of 0·28 to 0·62 in the case of Colusa Weir). This improvement arises because seasonally early floods (e.g. in December and January) carry an abundance of sediment that has been temporarily stored as deposits within the main channel following the previous flood season (e.g. slumped banks).

Stations within Sutter and Yolo Bypasses exhibited regressions (resulting both from all available data and from Dec–Jan only) that were inadequate for prediction (insignificant parameters and low coefficients of determination). Therefore, we removed outliers that significantly influenced the regressions according to the studentized residuals and Cook's *D* statistic (Helsel and Hirsch, 1992). This step dramatically improved the predictive power of the regressions (e.g. from adjusted R^2 of 0·06 to 0·57 for Yolo Bypass).

We computed the error associated with the linear regressions used to estimate daily sediment concentration, corrected for bias associated with log transformation (Duan, 1983). We then propagated the daily errors to compute root mean squared error (RMSE) for each event load. Likewise, erosion/deposition RMSEs were obtained for budget calculations in each reach. Although suspended sediment concentration error estimates inherent in USGS data collection and processing procedures have been estimated at 5% for the Colorado River and 20% for the Little Colorado River (Topping *et al.*, 2000), estimates of error in sediment transport, erosion and deposition reported here only include propagated error in estimated rating parameters.

Since no sediment concentration data were available for Moulton and Fremont Weirs (Figure 2), we computed concentration in the water above the level of each flood weir (Figure 4) based on upstream concentration data (from [Butte City – for Moulton Weir] and [the average of Knights Landing, Feather River and Sutter Bypass weighted by discharge – for Fremont Weir]), using the Rouse equation (Rouse, 1937):

$$Cs_i(z) = Cs_i(a)\left(\frac{h-z}{z}\frac{a}{h-a}\right)^{\frac{\omega_i}{\beta\kappa U_*}} \quad (1)$$

where

$$U_* = \sqrt{ghS} \quad \text{for steady uniform flow} \quad (2)$$

$Cs(z)$ is sediment concentration as a function of height z above the bed, $Cs(a)$ is the sediment concentration at a reference flow depth (Figure 4), ω is settling velocity (computed for the geometric mean of each size class i for natural particles via the work of Dietrich (1982)), β is the ratio of momentum to mass transfer (assumed to be unity), κ is von Karman's constant (assumed to be 0.41), a is the reference flow depth, z refers to an arbitrary height in the flow, g is gravitational acceleration, h is total flow depth measured from the water surface to the channel bottom and S is slope approximated by the elevation difference between flow at the weir and the next available stage gauge within the bypass, divided by the distance (Figure 4). The latter approximation was necessary to account for the water surface slope over the drop structure in the absence of a calibrated hydraulic model. Since bypasses receive the majority of flow during floods, it is reasonable to assume that this is the relevant water surface slope keeping sediment in suspension in the Rouse number in Equations (1) and (2). The true shear velocity is probably higher than this approximated value, due to increased turbulence near the weir. The subscript i refers to parameters for a specified grain size class.

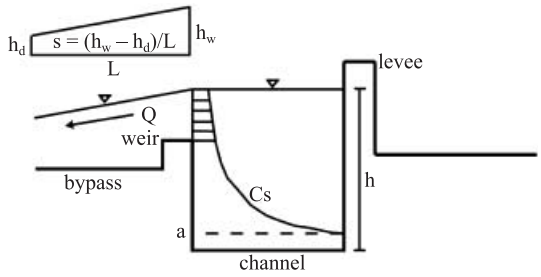

Figure 4. Schematic diagram of sediment concentration profile computation in flow above the height of a flood diversion weir. Concentration at flow depth, a, is computed using (3) and then plugged back into (1) to compute the concentration profile between a (assumed to be 75 mm above the bed) and the water surface. The resulting concentration profile is integrated to obtain concentration above weir level. Slope, s, is computed as the difference between h_w, the water surface elevation above the weir, and the next downstream gauge water surface measurement, h_d, divided by the distance along the flow direction, L.

Equation (1) is useful for predicting the sediment concentration profile when the reference concentration for a given depth is known. However, many sediment concentration data are published as mean concentrations (mg/l) or total (depth-integrated) concentrations with no indication of the concentration at a given depth. Therefore, we have inverted (1) to solve for the reference concentration 75 mm above the riverbed (the lower limit of depth-integrated sampling via DH-series sediment samplers employed by the USGS):

$$Cs_i(a) = \frac{\overline{Cs_i}}{\int_a^h \left(\frac{h-z}{z}\frac{a}{h-a}\right)^{\frac{-\omega_i}{\beta\kappa U_*}} dz} \quad (3)$$

where Cs_i is the fraction of the suspended load in the ith size class and the overbar indicates a depth-integrated value.

We then used the computed value of $Cs(a)$ to compute the concentration profile (Figure 4) for each grain size class using (1). These fractional (by grain size) computations utilized averages of suspended sediment grain size data from the relevant upstream stations. The resulting fractional concentrations were summed to obtain total daily concentrations. Our modeling approach for concentration does not explicitly account for particle interaction, density stratification or flocculation (McLean, 1992). Although these factors may have important implications for concentration profiles (see below), their effects cannot be determined *a priori*.

We obtained total event-based sediment discharge past each gauging point in the main stem, over each weir and through each bypass by integrating the multiple of discharge and sediment concentration (above weir-level for the bypass entries) over time. We evaluated net erosion/deposition in each reach by subtracting sediment effluxes from influxes.

DOI: 10.1002/esp

Table III. Comparison of event-based and long-term suspended loads and net reach erosion/deposition. The left-hand side of the table shows suspended loads for each station and the right-hand side shows net erosion/deposition for each reach. Left-hand columns: station (station codes from Figure 2); event-based suspended loads (Event) are total suspended loads for the 1964 event; long-term (LT) loads are annual averages computed by Singer and Dunne (2001); event load as a percentage of the annual average (% of LT); the maximum daily suspended load (Max Daily Qs) and the maximum daily sediment concentration (Max Cs). Right-hand columns: reach number corresponding to Figure 2; net event erosion (positive values)/deposition (negative values); long-term net erosion/deposition from Singer and Dunne (2001) and net event erosion/deposition as a percentage of the annual average (% of LT). Propagated RMSE values in suspended load associated with rating curve computations are given in parentheses. There are no errors for SA because sediment data were available for the 1964 event (refer to text). Table entries of 'n/a' refer to sites where no long-term estimates were made in the previous study. SU stands for Sutter Bypass and YO for Yolo Bypass (as entire reaches)

Suspended load (Mt)						Net reach erosion/deposition (Mt)			
Station	Event	Long-Term (LT)*&	% of LT	Max Daily Qs	Max Cs (mg/l)	Reach	Event	LT*	% of LT
BC	5·99(·044)	6·65	90	0·64(·014)	2155(48)	3	−2·66(·044)	−3·84	70
CC	2·45(·000)	n/a	n/a	0·50(·000)	8307(3)	4	0·28(·009)	0·36	78
CO	1·04(·003)	1·73	60	0·05(·006)	468(6)	5	2·27(·193)	n/a	n/a
CW	1·72(·003)	0·95	181	0·18(·001)	1099(7)	6	2·33(·007)	n/a	n/a
FR	1·62(·020)	1·81	90	0·35(·011)	543(17)	5#	*4·60*	*0·88*	*523*
FW	5·09(·172)	n/a	n/a	0·95(·077)	1626(132)	SU	−1·83(·085)	n/a	n/a
KL	0·88(·008)	1·61	55	0·03(·001)	477(22)	YO	−6·29(·172)	n/a	n/a
MW	0·57(·005)	n/a	n/a	0·12(·003)	2020(45)				
SA	2·91	4·30	68	0·47	1960				
SB	0·90(·085)	0·71	127	0·09(·029)	315(106)				
TW	0·44(·000)	0·35	126	0·03(·000)	572(2)				
VE	0·58(·007)	n/a	n/a	0·02(·001)	126(8)				
YB	1·25(·002)	n/a	n/a	0·15(·001)	239(2)				

* Values from Singer and Dunne, 2001.
& LT load estimates are unavailable (n/a) for stations where no computations were made in Singer and Dunne, 2001.
# For direct comparison with long-term (Singer and Dunne, 2001), value for Reach 5# was obtained by combining eros./dep. from 5 and 6.

Results: Suspended Load

Figure 2 shows computed suspended sediment discharge totals for the 1964 event at all gauges in and around the bypass system. Table III contains the errors associated with these computations, as well as comparisons between event-based (this study) and long-term (from the work of Singer and Dunne (2001)) washload and net erosion/deposition for main-stem reaches. Event-based suspended sediment discharge is consistent with long-term patterns characterized by Singer and Dunne (2001) (Table III), which computed mean annual efflux from the main stem via diversions from mean daily sediment discharge records. Suspended load during the 1964 event generally makes up 0·6–1·8 times annual totals (for sites where data were available in the prior study), indicating that a single flood's suspended load can be quite variable through the fluvial system, depending on its source, and it may comprise more than the average annual load.

Calculations for event-based suspended sediment transport into flood bypasses indicate that Colusa and Tisdale Weirs exceed average values (Table III), suggesting a large impact of the 1964 event on sediment delivery to Colusa, Tisdale and Sutter Bypasses. In summary, the high suspended flux at Butte City is mostly shunted out into Sutter Bypass by weirs, such that fluxes of both sediment and water at downstream main-stem stations are lower than average, while those over weirs are higher than average. Such a scenario for exporting sediment to bypass floodplain is apparently systematic during large floods.

Modeled efflux over Fremont and Moulton Weirs is also high. Fremont Weir, in fact, is the largest efflux term in the 1964-event sediment budget (>5 Mt), consistent with its high discharge (Figure 3), and only Butte City had a higher flux during the flood period. The suspended sediment flux calculations also indicate relatively high suspended sediment load at Cache Creek (Tables I and III), which derives large sediment loads from a basin of weak rocks, steep slopes and badlands (Lustig and Busch, 1967) and was the site of extensive mining of cinnabar for mercury used in gold extraction in the Sierra Nevada foothills. Conversely, relatively low transport was computed for the Feather River gauge, which is surprising considering the large flood pulse recorded at that station in late December (Figure 3). However, the sediment rating curve regression constructed for Feather River employed data from much smaller flows than that during the 1964 event (Tables I and II) and its upland basin appears to undergo episodic erosion during the largest floods (Table IV), for which no sediment data exist. As such, the flux into Reach 5 and over Fremont Weir (see calculation above) is probably a low estimate.

We tested model sensitivity to slope by adjusting S in (2) over Fremont Weir over an order of magnitude. This exercise resulted in a less than twofold change in sediment discharge over the weir for the 1964 event, indicating that these estimates are relatively robust.

Results: Net Reach Erosion/Deposition

Modeled event-based net erosion/deposition (divergence) of suspended load in main-stem reaches suggests deposition equivalent to ~0·7 times annual averages in Reach 3 and erosion 5·2 times average annual averages in Reaches 4 and 5, increasing downstream (Table III). The high suspended load erosion computed for Reach 5 is dominated by the most critical junction in the Sacramento network – the intersection of Feather River, Sutter Bypass, Sacramento River and Fremont Weir (gray rectangle in Figure 2). In particular the high flux of sediment (and water) over Fremont Weir correlates with net erosion for the reach as a whole, about half of which occurs upstream of Verona

DOI: 10.1002/esp

Table IV. The four largest flood peaks on record in the Sacramento bypass system: 1955, 1964, 1986 and 1997. The flood peak for 2006 at Fremont Weir is shown for comparison. All values are mean daily flow in m^3/s. 'N/A' signifies a year for which data were not available. The 1986 flood caused a gauge failure at Fremont Weir before the peak arrived

Station	1955	1964	1986	1997	2006
Butte City	4106	3455	4021	N/A	
Cache Creek	620	697	598	544	
Colusa	1093	1231	1062	1362	
Colusa Weir	1713	1917	N/A	N/A	
Feather River	8864	7391	N/A	N/A	
Fremont Weir	7250	6740	10054*	9426	5807
Knights Landing	753	767	N/A	N/A	
Moulton Weir	697	680	N/A	N/A	
Sacramento	2554	2798	3257	3200	
Sutter Bypass	N/A	3228	N/A	N/A	
Tisdale Weir	615	509	N/A	N/A	
Verona	1982	2090	2614	2549	
Yolo Bypass	6514	7335	10393	8468[&]	

* estimate of peak from CDWR.
[&] estimate of peak from USGS.

Table V. Deposition depths in Yolo Bypass based on various datasets. Each of the presented figures was calculated as an areal average, where the deposit volume was normalized by the particular area of the bypass over which it was measured. Excavated material depth estimates (from California Department of Water Resources (1991)) are averages calculated by dividing excavated volumes by estimated depositional area. Thus, each 'Excavated material' entry represents a different location in Yolo Bypass

Data Source	Deposition (cm)	Year(s)
Sedimentation pads	2	2006
Model calculations	85	1964
Cores	26	1997
Excavated material	104	1986–91
Excavated material	157	1986
Excavated material	62	1987
Excavated material	134	1991

and half downstream (Figure 2). However, as suggested above, a higher Feather River suspended load calculated using complete data could decrease (if not negate) computed erosion for Reach 5.

The net erosion/deposition results for the 1964 event indicate substantial net deposition in both bypasses. For example, the computed deposition from the event, if evenly distributed over the bypass (assuming a floodplain bulk density of 1·5 t/m^3), results in ~12 cm of vertical accretion in Yolo Bypass (assuming all sediment from Cache Creek is trapped in the settling basin upstream of Yolo Bypass) and ~4 cm in Sutter Bypass (assuming all sediment discharged over Moulton Weir is deposited in Butte Basin and all that discharged over Colusa and Tisdale Weirs is conveyed through their respective bypasses into Sutter Bypass). However, there is no basis for assuming that deposition is spatially uniform throughout a bypass. It is a known fact that large volumes of sediment have deposited immediately downstream of each flood weir, resulting in a topographic signature of splaylike lobes dissected by crevasses (Singer *et al.*, 2008). There is a need, therefore, to better understand sedimentation patterns and processes during floods.

Bypass Sedimentation

A sequence of alluvial splay deposits has been mapped along the margins of the Sacramento River (Robertson, 1987), similar to those observed at levee breaches elsewhere in the Central Valley (Florsheim and Mount, 2002, 2003). Several of these were incorporated into the modern flood control system and excavated as the sites for lateral weirs. In spite of efforts to remove the topography of such splays, deposition continues around the weir-controlled entrances to the flood bypasses, necessitating campaigns of sediment excavation by the CDWR. For example ~$2{\cdot}6 \times 10^6$ m^3 of sediment were removed from upstream portions of Yolo Bypass alone between 1986 and 1991 (California Department of Water Resources, 1991). This amounts to the removal of 100 cm depth of sediment if averaged over the excavated area that lies within the zone of splay topography (Table V). Excavation downstream of the weir in Figure 5 (Table V) likely removed sediment deposited during the 1964 event. This complex topography challenges our capability to realistically model sedimentation patterns, as has been accomplished with simple models (see, e.g., Moody and Troutman, 2000). Therefore, we pursue an empirical approach to generalize the spatial patterns of deposition since the 1991 removal of sediment from the upstream portion of Yolo Bypass. A large flood in 2006 serves as our representative event.

In order to better understand the pattern of topographic development associated with sedimentation, we worked with the CDWR to install within Yolo Bypass an array (regularized, with meter-scale randomization) of feldspar clay pads (Figure 5) that serve as stratigraphic markers above which the sedimentation from ensuing floods could be measured. Pads span a range of relative elevation and vegetative coverage and thus serve as representative sedimentation sites for particular regions of the bypass.

The flood peak of 2006 was ~86% of the 1964 peak, which is itself the third largest flood of record over Fremont Weir (Table IV). This recent flood, therefore, represents a significant flood from which to summarize spatial patterns of sedimentation in Yolo Bypass. Following the flood season, CDWR personnel returned to each pad location with GPS and cut a triangle several centimeters on a side into the deposit until they reached the marker horizon. They averaged depth measurements on the three sides of the triangle to determine the sedimentation rate. Sediment samples were analyzed for grain size at the University of Washington.

We averaged the pad sedimentation values from a relatively simple region of the bypass (within the black box in Figure 5) to summarize the prevailing patterns. We chose this region to minimize complexity associated with the near-levee zone, the oxbow lake or downstream areas that may receive remobilized sediment. The results of the pad analyses, presented in Figure 6, demonstrate a pattern of increasing sedimentation with distance from the weir, reaching a peak, which is followed by a rapid decline. The sedimentation pattern mimics that of natural levees (Bridge, 2003), which are characterized by similar curves of elevation and sand content with distance away from the channel delivering sediment (Figure 6).

We also conducted a sediment coring campaign within the upper 3 km of Yolo Bypass in 2003 and 2005 (before the 2006 flood). The objective was to document and interpret spatial patterns of sedimentation over the past century. We used a methodology for ^{210}Pb geochronology on floodplains (He and Walling, 1996; Goodbred and Kuehl, 1998) that has been enhanced to allow for the resolution and dating of discrete

DOI: 10.1002/esp

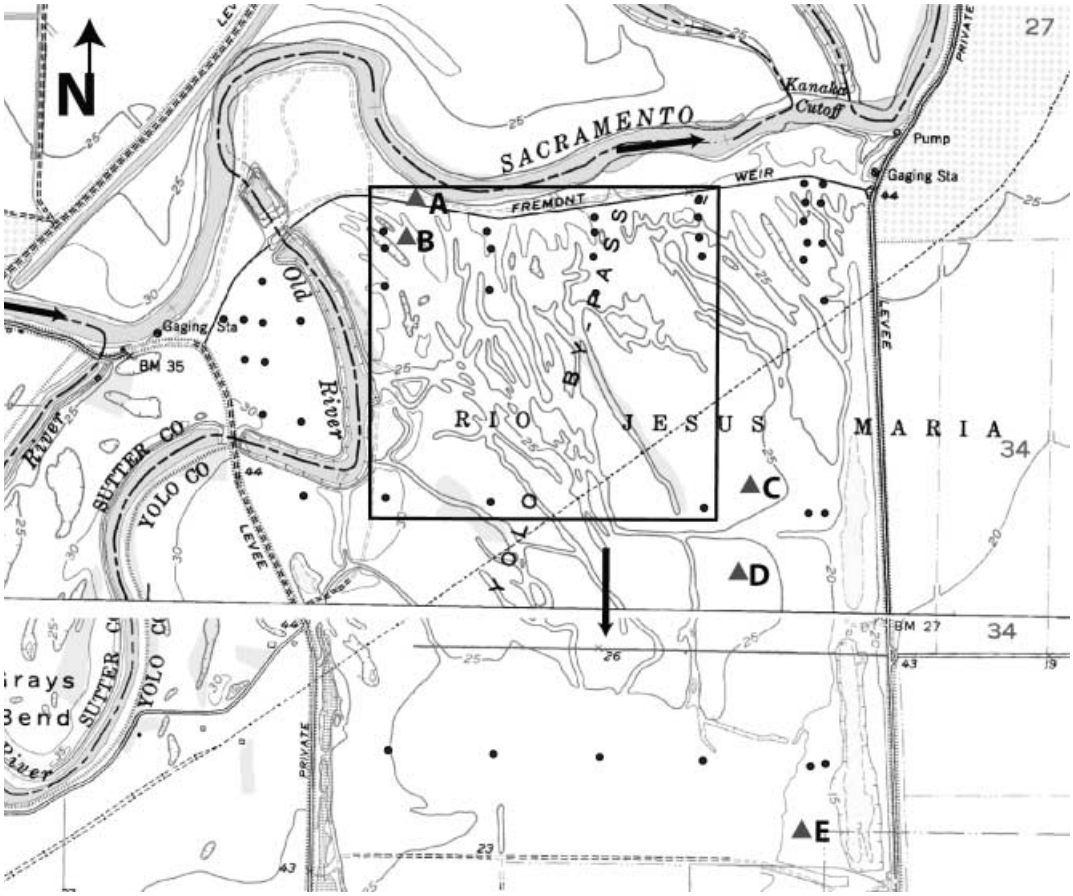

Figure 5. Topographic map (1:24 000) of Yolo Bypass entrance showing pad locations (black dots) and core locations (lettered triangles). The area is located at the box labeled 'Fremont Weir (FW)' in Figure 2. Thick black arrows indicate flow directions. The black square in the center of the bypass demarcates the pads used in analysis of sedimentation patterns at the bypass entrance. It avoids areas near the levees, the oxbow lake (labeled as 'Old River'), or downstream areas that may receive remobilized sediment from the up-bypass deposit. The entire upper region of the bypass depicted here is undisturbed by farming, regular vehicle traffic, grazing or any other perturbations, except for the well documented sediment removal excavations conducted every few decades in the upstream portions (upstream of core D). Map source: US Geological Survey.

sediment accumulation events (or continuous, if that is the dominant process) over the past 110 years (He and Walling, 1996; Goodbred and Kuehl, 1998; Aalto *et al*., 2003; Aalto *et al*., 2008). The 2·5 cm diameter cores were up to 5 m deep and were collected throughout the upstream end of Yolo Bypass. Processing of each core included X-radiography to document the preserved stratigraphy, granulometry to establish grain size patterns with planform location and depth and radiometric

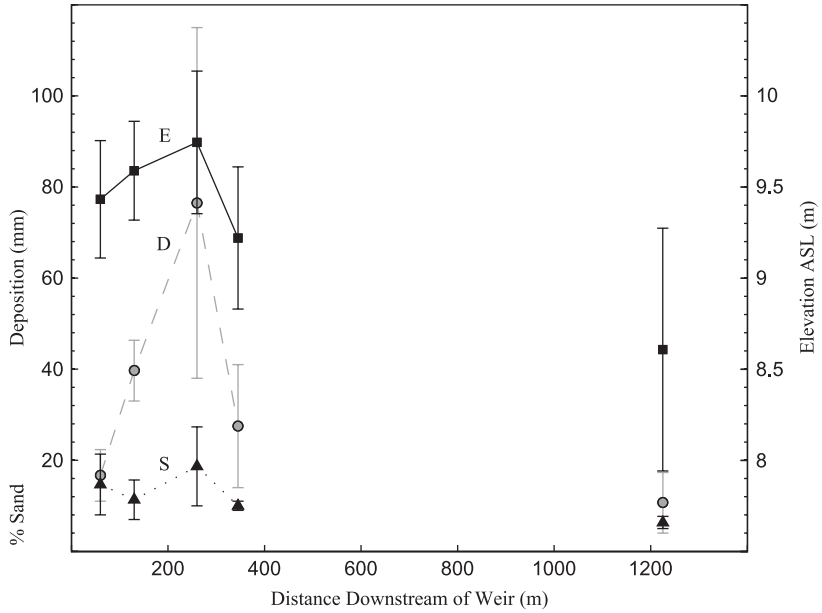

Figure 6. Elevation (E), pattern of deposition (D) in 2006 flood and sand content (S) for the same flood with distance downstream of the weir. The lines to 1200 m were not drawn due to lack of measurements over this relatively long distance. However, a monotonic decline is assumed. Error bars represent the range of all pads analyzed for a given distance.

DOI: 10.1002/esp

dating using adsorbed ^{210}Pb to date discrete deposition events. We measured the clay-normalized adsorbed excess activity (CNAXS), the difference between total measured activity of adsorbed ^{210}Pb, normalized by clay fraction, and the supported ^{210}Pb activity in the soil that results from the local decay of radon, the distribution of which is a strong function of soil depth. Excess ^{210}Pb arrives in two ways, by meteoric deposition onto the exposed soil surface, where it is absorbed within a few centimeters, and by emplacement of sediment deposits charged with excess ^{210}Pb activity from exposure in upstream soils. Because we have constrained the meteoric fallout rate of ^{210}Pb from the atmosphere at local undisturbed sites, we can estimate how long a particular meteoric cap has been growing from the total CNAXS activity (Aalto *et al.*, 2008). This provides age control on sedimentation packets exhibiting significant excess activity and for the surface exposure age of sites that have been scoured by a flood. We have developed an extensive core dataset for basin-wide sediment accumulation patterns and typical excess ^{210}Pb concentrations in flood-borne river sediment throughout the lower Sacramento basin (Aalto, unpublished data), which allows us to constrain the dates associated with ^{210}Pb concentrations exhibited for sediment deposits within Yolo Bypass with a temporal resolution of about five years.

Figure 5 shows a subset of coring locations from which we summarized sedimentation patterns that correspond to the spatial distribution of the sedimentation pads. The aforementioned sediment removal affected all cores except for Cores D and E. Figure 7 presents the CNAXS activity profile for Core E, which lies downstream of the aforementioned excavation area and demonstrates roughly what is expected if there is no net sedimentation detected. The profile is composed of an ingrown meteoric cap (zone of elevated activity from the surface to ~12 cm depth) that declines rapidly with depth to the background or supported level of ^{210}Pb in the soil. There is no obvious net sedimentation within this core and, based on the integral of excess activity within the cap, meteoric fallout has been in-growing since the mid-1980s, presumably because the large flood of 1986 (Table IV) scoured the surface of the bypass in this region (all cores presented here were collected before 2006, the largest flood since 1997).

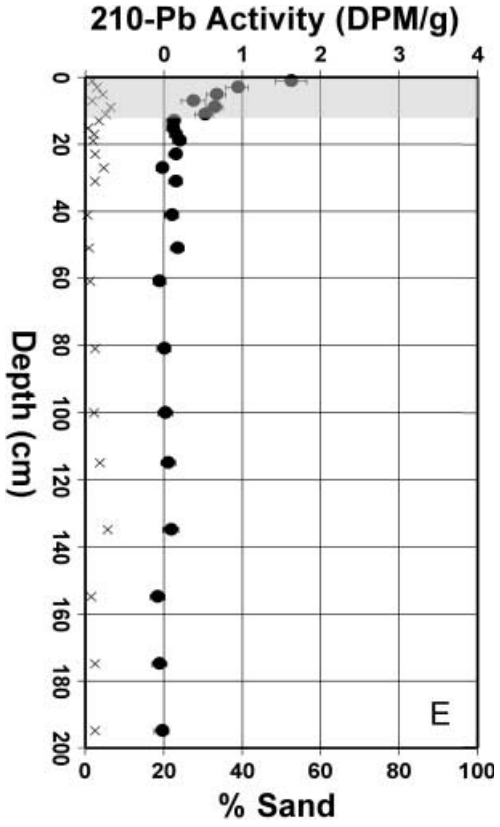

Figure 7. CNAXS ^{210}Pb activity profile of floodplain core E from Yolo Bypass (filled circles). Ingrowth of excess activity in the meteoric cap (top 12 cm) would take ~20 years at local fallout rates, signifying that the floodplain surface was 'reset' by scour in the mid-1980s. Sand content is depicted by '×'.

Figure 8 shows the CNAXS activity profiles for the remaining cores. Core A, located upstream of Fremont Weir (Figure 5), exhibits a sediment deposit of ~30 cm, with a level of CNAXS activity both in the sediment and represented by the ingrown meteoric cap (Aalto *et al.*, 2008) that corresponds to the late 1990s. This deposit, likely from the large 1997 flood, is topped vertically by a truncated meteoric cap that was buried by sediment from a small ~4 cm depositional event upon which a new cap has begun to grow (likely deposits from a smaller flood in the early 2000s). Core B contains a ~30 cm deposit of similar age overlain by a buried meteoric cap and a smaller ~8 cm deposit with a newer cap. The same temporal sequence is repeated in Core C, although the primary deposit in this core is thinner (~22 cm) and the secondary (more recent) deposit is thicker (~16 cm). Core D, farther down the bypass (Figure 5) barely exhibits the older depositional event from the late 1990s, but has a secondary deposit similar in size (~12 cm) to that of Core C. Following the downstream sequence, Core E, as previously discussed (Figure 7), reflects an environment of net erosion, rather than deposition. Detailed analysis of grain size distributions for the cores mimics the sand content pattern present in the sedimentation pad data. Sand content tends to decrease dramatically between Cores A and B, suggesting net deposition of larger size fractions present in the suspended load on the upstream side of the weir. The sand content decreases again from Core B to Core C, and then more gradually downstream of Core C to a background level of 5% at Core E. The downstream decrease in sand percentage may reflect the conveyance and deposition mechanics of sediment entering the bypass, as has been argued for sediment transport across natural levee systems (see, e.g., Bridge, 2003; Adams *et al.*, 2004).

Discussion

The sedimentation data from the pads and cores indicate that large floods entering the bypass carry high sediment loads, mobilized under short times to peak and long drawdown times (Table I), and drop most of their sediment load upstream and downstream of the weir. Both datasets indicate laterally continuous deposition blanketing a wide region near the weirs, for floods in 2006 (pads), early 2000s (cores) and the large 1997 flood (cores) – this picture is also consistent with the distribution of sediment removal efforts conducted after the 1964 and 1986 floods (J. Nosacka, CDWR, personal communication). However, after sufficient distance downstream from the weir, no net sedimentation occurs (see, e.g., Core E), and indeed there is evidence that the downstream bypass surface may be scoured by the largest floods flowing over them (Figure 7).

Our analyses and sedimentation data suggest that the largest floods (Table IV) tend to be responsible for most of the geomorphic change in Yolo Bypass. For example, the sedimentation in Yolo Bypass consists of decimeter-scale deposition during the moderate flood of 2006, and deposition of several decimeters during the large flood of 1997. Deposition probably occurred to similar depths (decimeter to meter scales) in the large

DOI: 10.1002/esp

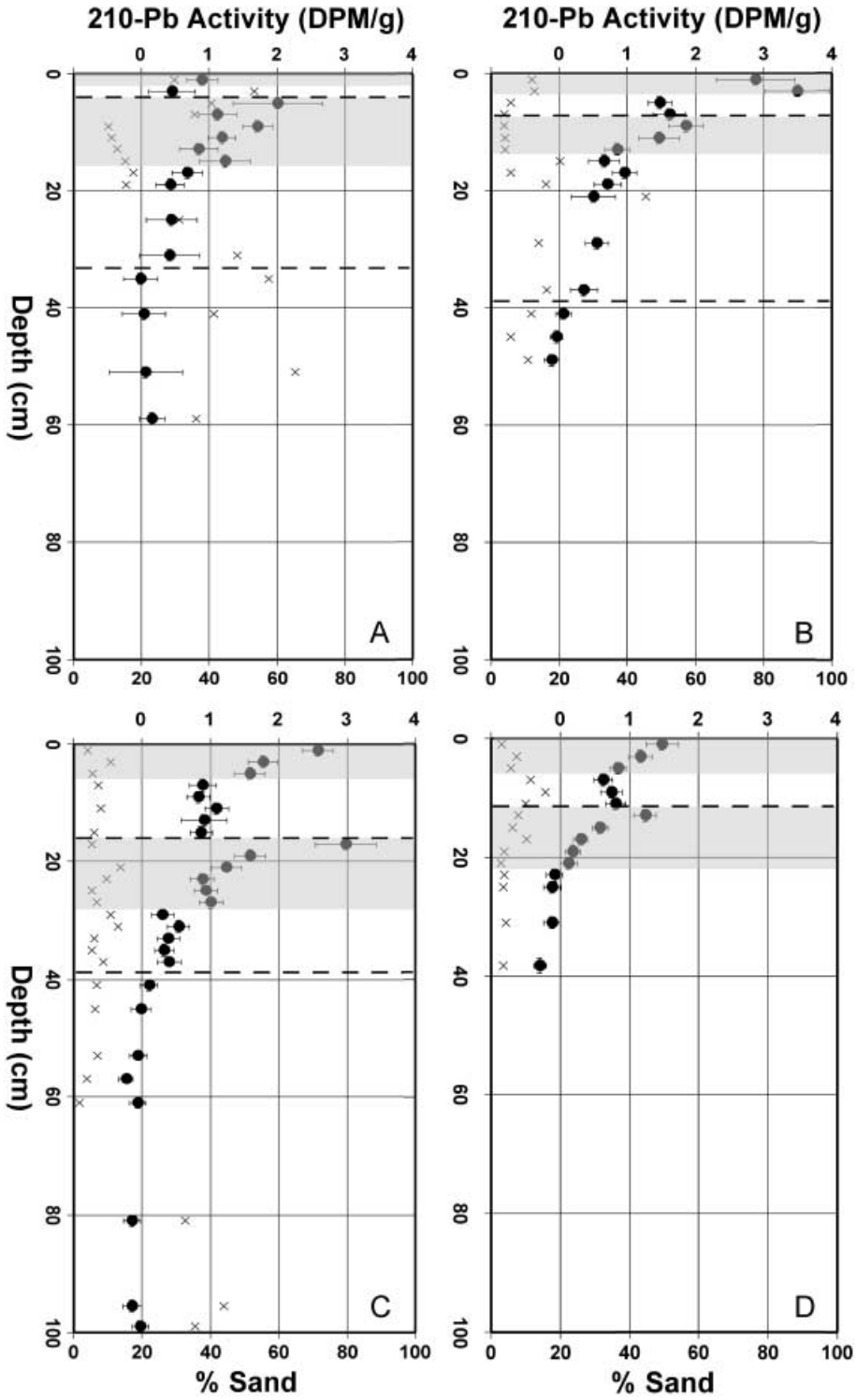

Figure 8. CNAXS ^{210}Pb activity profile of floodplain cores A–D from Yolo Bypass. Meteoric caps are shaded gray; transitions between sediment deposits are depicted with a dashed line. Locations are depicted in Figure 5, with the deposition signal discussed in text. Symbols are the same as in Figure 7.

floods preceding the sediment removal period. For example, dividing the 0·8 m of sediment removal between the other major floods since bypass construction (i.e. 1955, 1964 and 1986) yields 20–30 cm of deposition per flood (Table V). This deposition is primarily confined to a relatively small region near the entrance to the bypass that tends to promote further deposition in subsequent floods due to a feedback with the increasing development of the splay topography. Indeed, the depositional surface has built up since the last sediment removal (Singer and Dunne, 2004; Singer *et al.*, 2008), such that another sediment removal campaign was required in the autumn of 2006.

The entrance to each flood bypass can be thought of as a special case of a natural levee. Previous work on natural levees (e.g. Cazanacli and Smith, 1998; Aalto *et al.*, 2003; Bridge, 2003; Hudson and Heitmuller, 2003; Adams *et al.*, 2004) documents high rates of deposition close to the channel, relatively steep slopes between the crest of the levee and the surrounding flood basin, and concomitantly abrupt textural declines. Cazanacli and Smith (1998) described how the steepness of

DOI: 10.1002/esp

the leeward levee slope is inversely related to levee width, and that levees become broader with continual overbank deposition of progressively finer sediments because of depletion of coarse grain sizes transferred overbank. Adams *et al*. (2004) highlighted that broad, gently sloped levees with gradual declines in sediment size were formed by advective transport, which occurs when there is 'appreciable elevation head between the channel and its floodbasin'. Such a mechanism for advective transport would occur in an aggraded physiographic environment of a fluvial system crossing a large surrounding flood basin, such as the Sacramento Valley, where the river levees rise substantially above the surrounding floodplain. This formational mechanism contrasts with that of natural levees built by the turbulent diffusion of sediment over bank (Cazanacli and Smith, 1998; Aalto *et al.*, 2008).

The flood weir, over which flow and suspended load must be transported, may be conceptualized as a local perturbation that interrupts natural levee formation, thereby breaking the levee into two parts: a proto-levee upstream and an elongated, low-amplitude main levee downstream of the flood weir (Figures 9 and 10). The levee-building process essentially begins anew downstream of the flood weir, where sedimentation occurs once the flow loses energy downstream of the drop structure. The proto-levee is akin to an incomplete natural levee with high sand content (up to 50%) and a sedimentation peak that backs up against the flood weir. The downstream levee is broader, with a moderately defined topographic peak and lower sand content (up to 20%). Downstream of the peak, this surface downgrades gradually in slope and grain size (to a maximum of 10% sand at the downstream end). A positive feedback may develop on both levee surfaces, such that floods carrying sediment drop a portion of their load upstream of the topographic rise, itself formed by sedimentation from previous floods. This is illustrated in the plot of average deposition measured from the array of feldspar clay pads in Yolo Bypass (Figure 6) at the end of flooding in 2006 and in the core data (Figures 7 and 8 and Table V).

Downstream of this depositional zone, the topography is simple and flat. This area, low in sand content (maximum of 5%), appears to confirm Gilbert's hypothesis about efficient sediment conveyance through the bypasses. However, the ample evidence from various sources (i.e. sedimentation pads, sediment cores, sediment removal, topography, surface grain size) of net sediment accumulation near the weirs during large floods (Tables IV and V) adds complexity to Gilbert's concept of the bypass system as a self-scouring system with minimal storage.

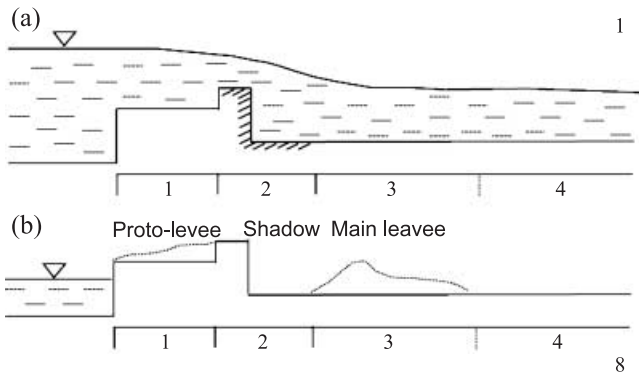

Figure 9. Schematic diagram of sediment laden flow over a weir at the beginning of a flood (a) and the resulting deposits after the flood (b). The floodplain is divided into four zones. Zones 1 and 3 exhibit net sedimentation, consisting of the proto-levee and the main levee, respectively. Zones 4 and 2, comprising the hydraulic shadow, exhibit no net sedimentation.

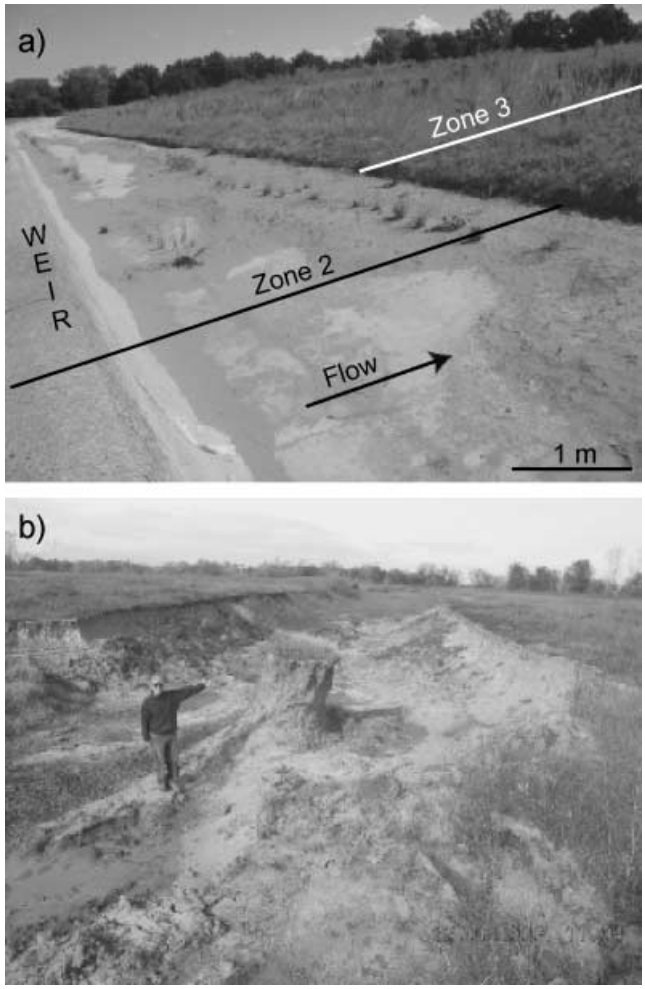

Figure 10. (a) Photo of Fremont Weir leading to Yolo Bypass after the 2004 flood season. Lag deposits are visible on the drop structure (Zone 2), and the upstream portion of the hydraulic shadow (Zone 3) is shown. (b) Headward erosion of prior sediment deposits at the downstream end of Zone 3 (hydraulic shadow) within Yolo Bypass. The view is upstream (north) toward Fremont Weir.

When subcritical flow from the main channel encounters an abrupt rise in the channel bottom (e.g. at a flood weir), flow depth decreases and velocity increases. Weirs are generally designed to force flow into a supercritical state at some point over the weir during flooding. A subsequent transition back to subcritical flow downstream of the weir is associated with flow separation and energy loss (Dingman, 1984), which is augmented by the engineered concrete armoring of the scour zone downstream of the weir. Therefore, the capacity of the flow to maintain sediment in suspension declines downstream of this hydraulic jump, which results in rapid sediment deposition downstream of the drop structure. This effect has been hypothesized to explain observed grain sizes in turbidity current deposits (Hiscott, 1994) and increased settling along the continuum from high capacity to low capacity conditions in laboratory suspension experiments (Cellino and Graf, 1999). It can result in the rapid settling of a wide range of grain sizes because local water surface slope is essentially zero, leading to an exceedance of the threshold for settling (e.g. in the ratio of settling velocity to shear velocity in the work of Kneller and McCaffrey (1999)), as the denominator (fluid shear) approaches zero. We hypothesize that the weir thus imposes a 'hydraulic shadow', or zone of no sedimentation, followed by a selective zone of sedimentation with a length that varies according to

DOI: 10.1002/esp

discharge, sediment concentration, grain size and evolving local topography. Downstream the flow becomes more uniform, the coarse sediment has mostly deposited and therefore there is limited sediment deposition (although scour is possible).

This is illustrated in Figures 9 and 10, which demarcate zones of net sedimentation (1 and 3) and zones of no net sedimentation (2 and 4) or scour. Zone 1 receives net sedimentation when sediment-laden flows go overbank (out of the river channel), but do not substantially overtop the weir. In addition, the topography built up by such sedimentation induces further deposition in subsequent floods, whether or not the weir is overtopped. Zone 2 corresponds to the hydraulic shadow of the weir at the drop structure, which is generally armored by concrete or riprap and will accumulate sediment only temporarily (e.g. at the tail end of a flood, Figure 10(a)). However, little net sedimentation is likely in Zone 2, due to the high turbulence from the hydraulic jump at the drop structure, sediment supply exhaustion during floods and swift evacuation of sediments on the rising limb of the hydrograph. Zone 3 receives net sedimentation due to the hydraulic effects previously discussed. This zone may be longer with increases in sediment concentration and suspended load grain sizes, and shorter with increases in discharge (i.e. through dilution). As was described for Zone 1, the increasing topographic expression of prior Zone 3 deposits will force a backwater effect that augments sedimentation during subsequent events, a positive feedback that is becoming increasingly relevant to flood control managers of Fremont Weir. Relatively small floods or those with low sediment load may induce erosion at the downstream end of Zone 3 that propagates headward toward the weir (Figure 10(b)).

Intriguingly, the historically documented processes of splay development along the Sacramento River are still active, albeit altered in their character by the flood control system. Suspended load carried by the Sacramento River now exits the river channel at fewer loci (Singer *et al.*, 2008), a focused sediment flux that could potentially produce larger deposits at the entrance to each bypass than would occur under natural conditions at those same locations. Likewise, the confinement of the levees on each side of the bypass further affects the spatial extent of the deposits, leading to a longer depositional zone emplaced within a narrower swath than would form under natural conditions.

Implications and Conclusion

The morphodynamic patterns of bypass sedimentation add complexity to Gilbert's hypothesis for efficient sediment conveyance through the bypass system. While Gilbert's concept of total sediment conveyance may apply to some areas of the bypass system, there is indeed localized sedimentation upstream and downstream of flood weirs, which are especially sensitive locations in terms of their impact on flood conveyance. Singer and Dunne (2004) and Singer *et al.* (2008) documented how this pattern of sediment deposition at the entrance to a bypass could impair the flood control system such that larger floods would be delivered to the lower Sacramento River channel. Field evidence also suggests that sediments deposited in Zone 3 of Yolo Bypass are being remobilized and evacuated (Figure 10(b)), ultimately depositing in locations farther downstream than Core E, which may be of concern if they contain legacy contaminants from 19th century hydraulic mining.

In terms of the general geomorphic understanding of levee construction, this research documents the active infilling of portions of Sacramento Valley bypasses by physical sedimentary processes that are analogous to natural levee building by advective overbank transport. Such an engineered, meticulously monitored 'levee laboratory' affords unique insight into how these important mechanisms are affected by perturbed and/or changing boundary conditions such as sediment supply, geometry and the frequency of large floods. The Sacramento bypass system provides opportunities to study how processes of natural levee formation may vary as channel-floodplain topography evolves over geologic time.

Acknowledgements—We would like to acknowledge Eric Buer and Jeff Nittrouer for significant contributions to field and laboratory work; Douglas Allen, Ned Andrews, Tom Dunne, Mark Hilles, Allan James, Nina Kilham, Daniel Malmon, Tony Pellegrini, Joel Rowland, Johnny Sanders, Mark Salak, Rebecca Wilhelm and Elowyn Yager for field assistance; Eliza Ghitis, Guenna Smith and Christie Leff for laboratory assistance; Charles Nittrouer for advice and access to laboratory facilities; Douglas Allen for GIS analysis; and support from the CALFED Bay-Delta Program (Grant 4600002659) and the National Science Foundation (Grants 0521663, 0403722 and 0521774). Development of the 210-Pb geochronology was supported in part by NSF Grants 0403722 and 0403722. We also are indebted to Trevor Greene of CDWR, who painstakingly emplaced and subsequently sampled the sedimentation pads, and Marianne Kirkland (CDWR), who made the pad study happen. Robb Jacobson and an anonymous reviewer provided helpful comments that improved the paper and Rudy Slingerland and Mike Church contributed to improvement of a previous version. Part of this research was performed while Singer held a National Research Council Research Associateship Award at USGS Menlo Park.

References

Aalto RE. 2002. *Geomorphic Form and Process of Mass Flux Within an Active Orogen: Denudation of the Bolivian Andes and Sediment Transport and Deposition Within the Channel-Floodplain Systems of the Amazonian Foreland*, Ph.D. thesis. University of Washington: Seattle, WA.

Aalto R, Lauer JW, Dietrich WE. 2008. Spatial and temporal dynamics of Strickland River floodplains during the past century. *Journal of Geophysical Research – Earth Surface* **113**: F01S04. DOI: 10.1029/2006JF000627

Aalto R, Maurice-Bourgoin L, Dunne T, Montgomery DR, Nittrouer CA, Guyot JL. 2003. Episodic sediment accumulation on Amazonian flood plains influenced by El Nino/Southern Oscillation. *Nature* **425**: 493–497.

Adams PN, Slingerland RL, Smith ND. 2004. Variations in natural levee morphology in anastomosed channel flood plain complexes. *Geomorphology* **61**: 127–142.

Asselman NEM. 2000. Fitting and interpretation of sediment rating curves. *Journal of Hydrology* **234**: 228–248.

Asselman NEM, Middelkoop H. 1995. Floodplain sedimentation: quantities, patterns and processes. *Earth Surface Processes and Landforms* **20**: 481–499.

Bridge JS. 2003. *Rivers and Floodplains, Forms, Processes, and Sedimentary Record*. Blackwell: Oxford.

California Department of Water Resources. 1991. Fremont Weir Sediment Removal Contract C50933, Specification 91-20, edited.

Cazanacli D, Smith ND. 1998. A study of morphology and texture of natural levees–Cumberland Marshes, Saskatchewan, Canada. *Geomorphology* **25**: 43–55.

Cellino M, Graf WH. 1999. Sediment-laden flow in open-channel under noncapacity and capacity conditions. *Journal of Hydraulic Engineering* **125**: 455–462.

Dietrich WE. 1982. *Flow, Boundary Shear Stress, and Sediment Transport in a River Meander*. University of Washington: Seattle, WA.

Dingman SL. 1984. *Fluvial Hydrology*. Freeman: New York.

Duan N. 1983. Smearing estimate: a nonparametric retransformation method. *Journal of the American Statistical Assocociation* **78**: 605–610.

Ferguson RI. 1986. River loads underestimated by rating curves. *Water Resources Research* **22**: 74–76.

Florsheim JL, Mount JF. 2002. Restoration of floodplain topography by sand-splay complex formation in response to intentional levee breaches, Lower Cosumnes River, California. *Geomorphology* **44**: 67–94.

Florsheim JL, Mount JF. 2003. Changes in lowland floodplain sedimentation processes: pre-disturbance to post-rehabilitation, Cosumnes River, CA. *Geomorphology* **56**: 305–323.

Gomez B, Phillips JD, Magilligan FJ, James LA. 1997. Floodplain sedimentation and sensitivity: summer 1993 flood, Upper Mississippi River Valley. *Earth Surface Processes and Landforms* **22**: 923–936.

Goodbred SL, Kuehl SA. 1998. Floodplain processes in the Bengal Basin and the storage of Ganges–Brahmaputra river sediment: an accretion study using Cs-137 and Pb-210 geochronology. *Sedimentary Geology* **121**: 239–258.

He Q, Walling DE. 1996. Use of fallout Pb-210 measurements to investigate longer-term rates and patterns of overbank sediment deposition on the floodplains of lowland river. *Earth Surface Processes and Landforms* **21**: 141–154.

Helsel DR, Hirsch RM. 1992. *Statistical Methods in Water Resources*. Elsevier: Amsterdam.

Hiscott RN. 1994. Loss of capacity, not competence, as the fundamental process governing deposition from turbidity currents. *Journal of Sedimentary Research* **A64**: 209–214.

Horowitz AJ. 2003. An evaluation of sediment rating curves for estimating suspended sediment concentrations for subsequent flux calculations. *Hydrological Processes* **17**: 3387–3409.

Hudson PF, Heitmuller FT. 2003. Local- and watershed-scale controls on the spatial variability of natural levee deposits in a large fine-grained floodplain: Lower Panuco Basin, Mexico. *Geomorphology* **56**: 255–269.

James LA, Singer MB. 2008. Development of the lower Sacramento Valley flood-control system: an historical perspective. *Natural Hazards Review* **9**: 125–135.

Kelley R. 1998. *Battling the Inland Sea*. University of California Press: Berkeley, CA.

Kesel R, Dunne K, McDonald R, Allison K. 1974. Lateral erosion and overbank deposition on the Mississippi River in Louisiana caused by 1973 flooding. *Geology* **2**: 461–464.

Kneller B, McCaffrey W. 1999. Depositional effects of flow nonuniformity and stratification within turbidity currents approaching a bounding slope: deflection, reflection, and facies variation. *Journal of Sedimentary Research* **69**: 980–991.

Lustig LK, Busch RD. 1967. *Sediment Transport in Cache Creek Drainage Basin in the Coast Ranges West of Sacramento, California*, US Geological Survey Professional Paper 562-A. Washington, DC.

McLean SR. 1992. On the calculation of suspended load for noncohesive sediments. *Journal of Geophysical Research – Oceans* **97**: 5759–5770.

Middelkoop H, Asselman NEM. 1998. Spatial variability of floodplain sedimentation at the event scale in the Rhine–Meuse Delta, The Netherlands. *Earth Surface Processes and Landforms* **23**: 561–573.

Moody JA, Troutman BM. 2000. Quantitative model of the growth of floodplains by vertical accretion. *Earth Surface Processes and Landforms* **25**: 115–133.

Nanson GC, Croke JC. 1992. A genetic classification of floodplains. *Geomorphology* **4**: 459–486.

Robertson KG. 1987. *Paleochannels and recent evolution of Sacramento River, California*, masters thesis. University of California, Davis: Davis, CA.

Rouse H. 1937. Modern conceptions of mechanics of fluid turbulence. *American Society of Civil Engineers* **102**: 463–505.

Siggers GB, Bates PD, Anderson MG, Walling DE, He Q. 1999. A preliminary investigation of the integration of modelled floodplain hydraulics with estimates of overbank floodplain sedimentation derived from Pb-210 and Cs-137 measurements. *Earth Surface Processes and Landforms* **24**: 211–231.

Singer MB. 2007. The influence of major dams on hydrology through the drainage network of the Sacramento Valley, California. *River Research and Applications* **23**: 55–72.

Singer MB, Dunne T. 2001. Identifying eroding and depositional reaches of valley by analysis of suspended-sediment transport in the Sacramento River, California. *Water Resources Research* **37**: 3371–3381.

Singer MB, Dunne T. 2004. An empirical-stochastic, event-based model for simulating inflow from a tributary network: theoretical framework and application to the Sacramento River basin, California. *Water Resources Research* **40**: W07506. DOI: 07510.01029/02003WR002725

Singer MB, Dunne T. 2006. Modeling the decadal influence of river rehabilitation scenarios on bed-material sediment flux in a large river basin. *Water Resources Research* **42**: W12415. DOI: 10.1029/2006WR004894

Singer MB, James LA, Aalto R. 2008. Status of the lower Sacramento Valley flood-control system within the context of its natural geomorphic setting. *Natural Hazards Review* **9**: 104–115.

Sommer T, Harrell B, Nobriga M, Brown R, Moyle P, Kimmerer W, Schemel L. 2001a. California's Yolo Bypass: evidence that flood control can be compatible with fisheries, wetlands, wildlife, and agriculture. *Fisheries* **26**: 6–16.

Sommer TR, Harrell WC, Solger AM, Tom B, Kimmerer W. 2004. Effects of flow variation on channel and floodplain biota and habitats of the Sacramento River, California, USA. *Aquatic Conservation: Marine and Freshwater Ecosystems* **14**: 247–261.

Sommer T, Nobriga M, Harrell WC, Batham W, Kimmerer WJ. 2001b. Floodplain rearing of juvenile chinook salmon: evidence of enhanced growth and survival. *Canadian Journal of Fisheries and Aquatic Sciences* **58**: 325–333.

Stewart JH, LaMarche VC. 1967. *Erosion and Deposition Produced by the Flood of December 1964 on Coffee Creek Trinity County, California*, US Geological Survey Professional Paper 422-K. Washington, DC.

Swanson KM, Watson E, Aalto R, Lauer W, Dietrich WE, Apte S, Bera M, Marshall A, Taylor M. 2008. Sediment load and floodplain deposition rates: comparison of the Fly and Strickland rivers, Papua New Guinea. *Journal of Geophysical Research Earth Surface* **133**: F0I503. DOI:10.1029/2006JF000623

Ten Brinke WBM, Schoor MM, Sorber AM, Berendsen HJA. 1998. Overbank sand deposition in relation to transport volumes during large-magnitude floods in the Dutch sand-bed Rhine River system. *Earth Surface Processes and Landforms* **23**: 809–824.

Topping DJ, Rubin DM, Vierra JLE. 2000. Colorado River sediment transport 1. Natural sediment supply limitation and the influence of Glen Canyon Dam. *Water Resources Research* **36**: 515–542.

Trimble SW. 1974. *Man-Induced Soil Erosion in the Southern Piedmont, 1700–1970*. Soil Conservation Society of America: Ankeny, IA.

US Army Corps of Engineers. 1965. *Report on Floods of Dec. 1964, Jan. 1965*. Sacramento, CA.

US House of Representatives. 1911. Flood control – Sacramento and San Joaquin River systems, California. In *HR Document, No. 81, 62nd Congress, 1st Session, Washington, D.C.*, edited, p. 54.

Waananen AO, Harris DD, Williams RC. 1971. *Floods of December 1964 and January 1965 in the Far Western States*, US Geological Survey Water Supply Paper 1866-A. Washington, DC.

Wallace JM, Gutzler DS. 1981. Teleconnections in the geopotential height field during the Northern Hemisphere winter. *Monthly Weather Review* **109**: 784–812.

Walling DE. 1999. Using fallout radionuclides in investigations of contemporary overbank sedimentation on the floodplains of British rivers. In *Floodplains: Interdisciplinary Approaches*, Marriott SB, Alexander J (eds). Geological Society of London: London; 41–59.

Walling DE, Bradley SB. 1989. Rates and patterns of contemporary floodplain sedimentation: a case study of the River Culm, Devon, UK. *Geojournal* **19**: 53–62.